JOURNAL OF THERMOPHYSICS AND HEAT TRANSFER
Vol. 24, No. 4, October–December 2010

Investigation on Microheat Pipe Array with Arteries

Jian Kang,* Xin Fu,† and Weiting Liu‡
Zhejiang University, 310027 Hangzhou, People's Republic of China
and
Paolo Dario§
Scuola Superiore Sant'Anna, 56025 Pisa, Italy

DOI: 10.2514/1.49913

A novel design of microheat pipe array with arteries that can limit the onset of the dryout region is proposed. Additional pipes are inserted between adjacent microheat pipes to improve liquid transportation ability from the condenser section to the evaporator section. These additional pipes have smaller cross-sectional dimensions than the microheat pipe and serve as an artery of the microheat pipe. Because of the liquid pressure difference in the meniscuses between the two ends of the microheat pipe, an additional amount of working liquid can be effectively transported to the evaporator section through these arteries, which definitely improves the performance of the microheat pipe. The working principle and optimal design of the arteries are numerically investigated with a one-dimensional steady-state model of the artery microheat pipe array. To verify the idea, a silicon-based artery microheat pipe array and traditional microheat pipe sample with the same dimensional parameters are fabricated by lithographic technique and anodic bonding process. The validation has been carried out by the comparison observation experiments of the novel microheat pipe and the traditional microheat pipe through a microscopic camera. Both the model's numerical solution and the observation results indicate that the artery microheat pipe array can effectively extend thermal working range.

Nomenclature

A = liquid area in the V-groove of the microheat pipe, m^2
A' = area of the cross section, m^2
A'_L = liquid area in the cross section at the cold end ($x^* = 1$), m^2
a_A = width of the artery, m
a = width of the microheat pipe, m
B_1 = constant in expression for A_1
B_2 = constant in expression for $\mathrm{d}R^*/\mathrm{d}x^*$
c = constant in expression for a_1/a
f = friction factor
g = acceleration due to gravity, m/s^2
K' = constant in expression for τ_w
L = length of heat pipe, m
L_h = half of total wetted length, m
P = liquid pressure, N/m^2
P^* = nondimensional liquid pressure
P_R = reference pressure, N/m^2
Q = heat supplied to the liquid, W/m^2
R = radius of meniscus curvature in the V-grooves of the microheat pipe, m
R_0 = radius of meniscus curvature in the V-grooves of the microheat pipe at $x = 0$, m
R_L = radius of meniscus curvature in the V-grooves of the microheat pipe at $x = L$, m
R_R = reference radius of meniscus curvature, m
V = axial liquid velocity, m/s
V_A = liquid velocity in the artery, m/s
V^* = nondimensional liquid velocity
V_R = reference liquid velocity, m/s
x = coordinate along the heat pipe, m
x^* = nondimensional coordinate along microheat pipe
α = half apex angle of V-groove, rad
β = inclination of substrate with horizontal, rad
γ = contact angle, rad
δ = correction coefficient
η = fill charge
λ = latent heat of vaporization of coolant liquid, J/kg
μ = viscosity of coolant liquid, kg/ms
ρ = density of coolant liquid, kg/m^3
σ = surface tension of coolant liquid, N/m
τ_{wA} = shear stress between liquid and substrate of the artery, N/m^2
τ_w = shear stress between liquid and substrate of the microheat pipe, N/m^2
Φ = curvature, m^{-1}

Received 30 March 2010; revision received 20 June 2010; accepted for publication 27 June 2010.

*Ph.D. Candidate, State Key Laboratory of Fluid Power Transmission and Control.
†Professor, State Key Laboratory of Fluid Power Transmission and Control.
‡Associate Professor, State Key Laboratory of Fluid Power Transmission and Control.
§Professor, CRIM and ARTS Labs, Viale Rinaldo Piaggio 34.

I. Introduction

NOWADAYS, due to the fast improvement of the integration degree of microelectronic devices, micro scale heat dissipation is getting more and more attentions. Because microheat pipe (MHP) is able to uniform surface heat dissipation, lots of researches have been done in this field to investigate the working principle and the optimal design of the MHP. The concept of MHP was first proposed by Cotter [1] in 1984. According to his definition, the MHP is a hollow pipe with width of 10–500 μm and length of 10–20 mm; the cross-sectional shape of the MHP is commonly triangle or rectangle; liquid circulation is driven by the capillary force in the V-grooves. The operation mechanism of the MHP was studied by many researchers. Sobhan et al. [2] successfully used the Young–Laplace equation to describe the fluid dynamics of the MHP. They found that the cross-sectional design has a great effect on the MHP's transmission efficiency. Suman et al. [3] and Suman and Hoda [4] built a general steady-state model by using a macroscopic approach, and took the inertia of the flowing liquid and the liquid-solid friction force into account.

It was found that the dryout region will propagate in the evaporator section when the input heat flux exceeds the critical level. Dry-out

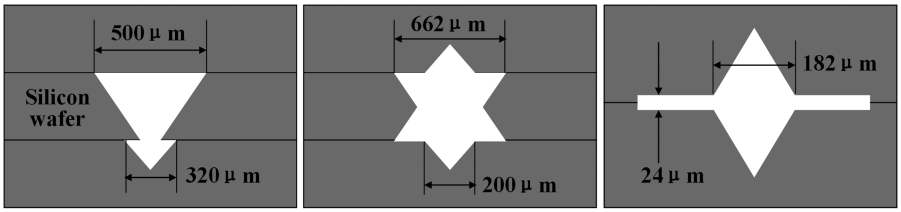

Fig. 1 Previously designed cross section of MHP: a) Berre's design, and b) and c) Kang's designs.

region [5] has a negative impact on the performance of the MHP, because it blocks the working liquid being transported to the evaporator section. To prevent the propagation of the dryout region, many methods have been used to enhance the efficiency of the liquid backflow. One of them is increasing the number of *V*-grooves in the MHP, as more *V*-grooves provide bigger capillary force for the working liquid backflow. Berre et al. [5] designed a kind of MHP with the artery pipe shown in Fig. 1a; Kang and Huang [6] designed the star grooves and rhombus grooves MHP shown in Fig. 1b and 1c. Besides those different designs of cross section of MHP, several different grooves were also proposed and fabricated with metal material as substrate, such as OMEGA groove [7,8] and swallow tailed groove [9], which can enhance the thermal performance of heat pipe. Unfortunately, it seems impossible to apply in our silicon-based MHP due to the difficulties of fabrication processes. On the other hand, a method of reducing the friction force in the MHP was proposed. A MHP heat spreader [10] was designed to allow liquid and vapor flow separately to reduce viscous force; Qu et al. [11] analyzed the effect of the functional surface [12,13] on improving the efficiency of the liquid backflow, as the functional surface can promote the movement of droplets. In addition, the concept of the electrohydrodynamically (EHD) augmented MHP was studied by Suman [14], as the EHD pumping can improve the heat transport capacity of MHP.

To test the thermal performance of the MHP and verify the proposed model, lots of experiments have been done. Kim et al. [15] measured the maximum heat transport rate and the thermal resistance, which has a good fitness with the numerical results. High-speed camera was introduced by Lin et al. [16] to record the working state of the microloop heat pipe. The temperature profile on the surface of the MHP array was deduced from the experimental results by Launay et al. [17]. However, the effect of all these methods is limited by the onset of the dryout region. Furthermore, their fabrication processes are complex and difficult to be applied. Most of the above mentioned studies are based on the working principle of a single MHP, which can only transport heat in one-dimensional direction. In practice, the MHP array is commonly used, and the collaboration between the adjacent pipes has been supposed to have a positive effect which needs further analysis.

In this paper, a novel artery MHP array is presented with the objective to enhance the liquid backflow. As shown in Fig. 2a, two smaller pipes which serve as arteries are positioned on the both sides of an ordinary MHP, and the two ends of the arteries and the MHP are connected together by two connecting pipes. Because of the two ends' pressure difference of the *V*-grooves in the MHP, the working liquid is transported to the evaporator section both through the MHPs' *V*-grooves and the arteries. A steady-state model of the artery MHP array is built to numerically investigate the effect of the arteries. The model's numerical solution is applied to verify whether this novel artery MHP array can effectively limit the onset of the dryout region. An artery MHP array prototype and an comparison MHP with the same size are fabricated on silicon wafer and tested through an experimental setup which is similar to the one proposed by Kim et al. [15]. Microscopic camera is used to check the working state of the artery MHP array. Validation is done both by numerical model investigation and experimental comparison between the two types of MHP through working state observation.

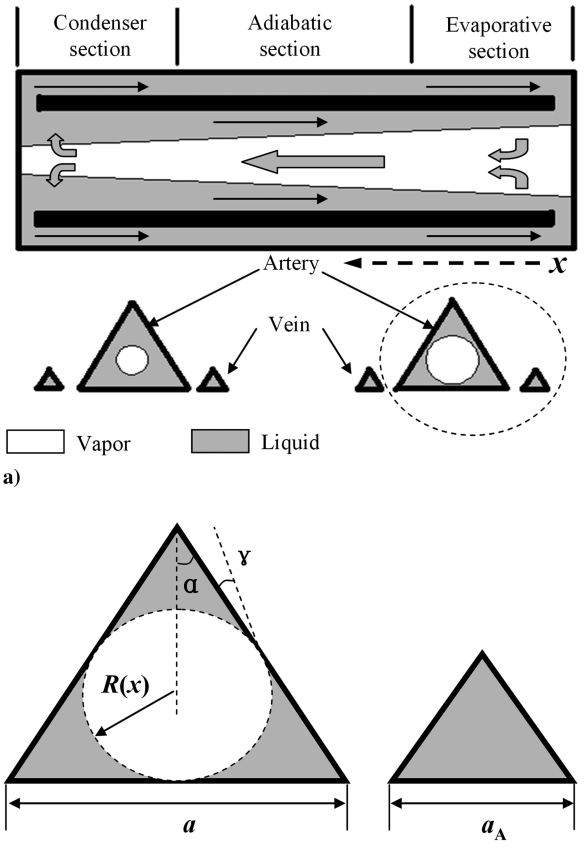

Fig. 2 Diagram of MHP and arteries: a) working principle of the artery MHP, and b) schematic diagram of the MHP and artery.

II. Modeling

The working principle of the novel artery MHP array is shown in Fig. 2a. The smaller artery pipes fully filled with working liquid are used to transport working liquid back to the evaporator section. The fully liquid occupying is guaranteed by the design of the different dimension of the MHP and its arteries which provides enough pressure difference between them and keeps the vapor off the arteries. The liquid evaporation and condensation effectiveness leads to different radius of meniscus formation between the two ends of the *V*-grooves in the MHP, which provides the arteries with driving force due to the capillary force difference between the two ends of the *V*-grooves.

As the cross-sectional dimensions of the artery MHP array are much smaller than its axial length, it is acceptable to describe the working states with a one-dimensional model. The following assumptions are employed in the modeling process:

1) Steady-state incompressible flow along the length for both the liquid and the vapor with constant physical properties.

2) The vapor is at saturated state.

3) The radius of the meniscus is constant at a given location in the MHP.

4) Uniform distribution of heat input.

5) The shear force between the liquid and vapor is neglected.

A. Working Principle of the Artery

In normal working state, the arteries are fully filled with working liquid. The liquid pressure difference between the two ends of the artery is the same as the pressure difference between two ends of the V-grooves in the MHP, as the two ends of them are connected. The Young–Laplace equation is used to calculate this liquid pressure difference. The following equation is used to describe the working state of the artery. The stress equation for the flowing liquid in the arteries is given by:

$$\sigma\left(\frac{1}{R_0}-\frac{1}{R_L}\right)-\frac{4(1+\sin\alpha)L\tau_{wA}}{ac\cos\alpha}+\rho g\sin(\beta)L=0 \tag{1}$$

The first item in Eq. (1) represents the driving stress, which is the pressure difference between the meniscuses in the two ends; the second term represents the shear stress between liquid and substrate; the last term represents the effect of gravity on the working liquid in the arteries. The liquid flow in the arteries is assumed to be the fully developed laminar flow. Therefore, the friction force between liquid and substrate can be given by:

$$\tau_{wA}=\frac{V_A K'\mu(\sin\alpha+1)}{2ac\cos\alpha} \tag{2}$$

In Eqs. (1) and (2), $c=a_A/a$ as shown in Fig. 2b, $K'=13.33$. Here, K' is a friction factor, which is a constant for a specific geometry (e.g., 13.33 for triangle) [18]. Thus, the liquid velocity in the arteries can be obtained in Eq. (3)

$$V_A=\frac{a^2c^2\cos^2\alpha\{\sigma(\frac{1}{R_0}-\frac{1}{R_L})+\rho g\sin(\beta)L\}}{2LK'\mu(1+\sin\alpha)^2} \tag{3}$$

B. Working Principle of the MHP

In the MHP, the direction of liquid and vapor flow assumed to be fully developed laminar flow is opposite. Suman et al.'s model [3] for fluid flow and heat transfer in V-groove of the MHP is here used to describe the liquid flow and heat transfer

$$\rho AV\frac{\mathrm{d}V}{\mathrm{d}x}+A\frac{\mathrm{d}P}{\mathrm{d}x}+2L_h\tau_w-\rho g\sin(\beta)A=0 \tag{4}$$

$$\frac{\mathrm{d}P}{\mathrm{d}x}-\frac{\sigma}{R^2}\frac{\mathrm{d}R}{\mathrm{d}x}=0 \tag{5}$$

$$\frac{\mathrm{d}}{\mathrm{d}x}(\rho VA)+\frac{Qa}{\lambda}=0 \tag{6}$$

$$\tau_w=\frac{VK'\mu R\cos(\alpha+\gamma)}{4A\sin\alpha} \tag{7}$$

The equation for the liquid flow in the V-groove is given by Eq. (4). Equation (5) is the differential form of Young–Laplace equation. It is assumed in Eq. (6) that all the input heat of MHP is used for evaporation. The friction between liquid and substrate is described in Eq. (7) with no concern about the friction between liquid and vapor. The differential form of liquid velocity and radius of meniscus can be obtained from the Eqs. (4–7), as follows:

$$\frac{\mathrm{d}V}{\mathrm{d}x}=\frac{\frac{aQ\sigma}{2B_1\rho\lambda R}+R^2V\rho g\sin\beta-V^2B_2}{\rho V^2R^2-\frac{\sigma R}{2}} \tag{8}$$

$$\frac{\mathrm{d}R}{\mathrm{d}x}=\frac{R^2\rho g\sin\beta+\frac{QaV}{B_1\lambda}-VB_2}{\sigma-2\rho V^2R} \tag{9}$$

In Eqs. (8) and (9), B_1 and B_2 are expressed by Eqs. (10) and (11)

$$B_1=\{\cot(\alpha+\gamma)-\phi/2\}+\frac{\cot(\alpha+\gamma)\cos(\alpha+\gamma)\sin\gamma}{\sin\alpha} \tag{10}$$

$$B_2=\frac{\mu K'\cos^2(\alpha+\gamma)}{2\sin^2\alpha(B_1)^2} \tag{11}$$

C. Boundary Conditions of the Artery MHP

As the two ends of the arteries and the MHP are connected together, the boundary conditions of the MHP can be obtained from the working states of the arteries. The liquid flow rate in the two ends ($x=0, x=L$) of the MHP have the same value as that in the adjacent arteries, but the liquid in the two ends of the MHP and the adjacent arteries flow in different directions. Therefore, the boundary conditions of the MHP at the two ends ($x=0,\ x=L$) can be expressed in Eqs. (12) and (13).

At

$$x=0,\qquad V=-\frac{a^2c^2V_A}{4B_1R_0^2\tan\alpha} \tag{12}$$

At

$$x=L,\qquad R=R_L=\delta R_R \tag{13}$$

D. Nondimensionalization

Equations (8) and (9) and the boundary conditions are non-dimensionalized using the parameters shown in Eqs. (14–16)

$$R^*=\frac{R}{R_R},\qquad R_R=\frac{a\sin(\alpha)}{2\cos(\alpha+\gamma)} \tag{14}$$

$$V^*=\frac{V}{V_R},\qquad V_R=\frac{QaL(1+\sin\alpha)}{\rho R_R^2\lambda\sin\alpha} \tag{15}$$

$$x^*=\frac{x}{L} \tag{16}$$

The model for the fluid flow and heat transfer in the artery MHP can be expressed by Eqs. (17) and (18)

$$\frac{\mathrm{d}V^*}{\mathrm{d}x^*}=\frac{\frac{aQ\sigma L}{2B_1\rho\lambda R^*R_R}+(R^*R_R)^2(V^*V_R)L\rho g\sin\beta-(V^*V_R)^2B_2L}{\rho(V^*)^2(V_R)^3(R^*R_R)^2-\frac{\sigma(R^*R_R)V_R}{2}} \tag{17}$$

$$\frac{\mathrm{d}R^*}{\mathrm{d}x^*}=\frac{(R^*R_R)^2\rho g\sin(\beta)L+\frac{aQV^*V_RL}{B_1\lambda}-V^*V_RB_2L}{\sigma R_L-2\rho(V^*V_R)^2R^*R_R^2} \tag{18}$$

The boundary conditions can be expressed by Eqs. (19) and (20) as

$$x^*=0,\qquad V^*=-\frac{a^2c^2V_A}{4B_1R_0^2V_R\tan\alpha} \tag{19}$$

At

$$x^*=1,\qquad R^*=\delta \tag{20}$$

E. Numerical Solution

An iterative procedure is used to solve the model. The integration process uses the method of Runga–Kutta fourth-order integration routines and starts with the inputs value of input heat, dimensions of the artery MHP and properties of the working liquid. First, a value of

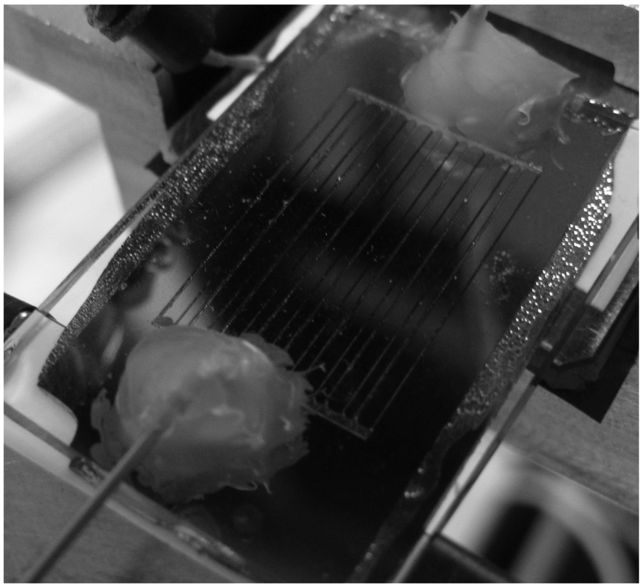

Fig. 3 Samples of the artery MHP array.

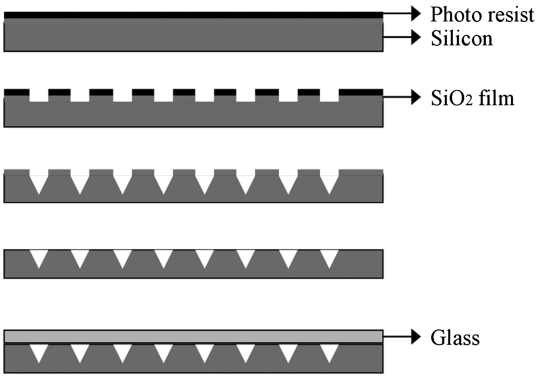

Fig. 4 Fabrication process.

R^* at $x^* = 0$ is assumed, then the only V^* at $x = 0$ can be obtained from the Eq. (3). If the value of R^* at $x^* = 1$ is not equal to δ, a new R^* at $x^* = 0$ is assumed. This kind of routine continues until $R^* = \delta$ within a tolerance limit at $x^* = 1$. It is found that satisfied results can be obtained with the step size 1.0×10^{-4}.

III. Structure and Fabrication Process

The artery MHP array in the plate is composed of 17 parallel triangular pipes. Among these pipes, 9 of them serve as MHP, 200 μm wide, 156 μm deep and 20 mm long, and the other 8 smaller pipes serve as artery between every neighbor MHPs, 100 μm wide, 78 μm deep and 20 mm long. At the two ends of these pipes, two connecting pipes are designed to connect all the pipes with the two filling holes drilled on the Pyrex glass. The artery MHP array plate is shown in Fig. 3. The diameter of these filling holes is about 1 mm. To validate the effectiveness of the novel design, an ordinary MHP array with exactly the same parameters is also fabricated.

As shown in Fig. 4, lithographic technique and anodic bonding process are used to fabricate this artery MHP array plate, and ethanol is selected as filling liquid.

IV. Experimental Facility and Working Conditions

To verify the working principle of the artery MHP array, an experimental setup for microscopic observation together with temperature measurement capability is constructed and shown in Fig. 5. The experimental apparatus simulates the working condition of a heat dissipation system with steady heat flux in the evaporator section and steady temperature in the condenser section.

A thin film resistance heater is adhered to the evaporator section by thermal grease to provide uniform heat flux, which is controlled by a DC power supply. *K*-type thermal couples and Pt-100 thermal resistances are used here for temperature measurement. At the condenser section, the MHP array is mounted on a plate heat sink. The steady temperature cooling liquid flow through the plate heat sink and take away the heat transferred through the MHP array. To inhibit the heat dissipation from the system to the air, the whole tests are carried out in a vacuum chamber.

To observe the working state of the MHP array, a high-speed camera and microscopic system (KEYENCE digital microscope system VHX-600) are mounted above the MHP array and take pictures through a glass observation window with amplification factor from 20 to 250.

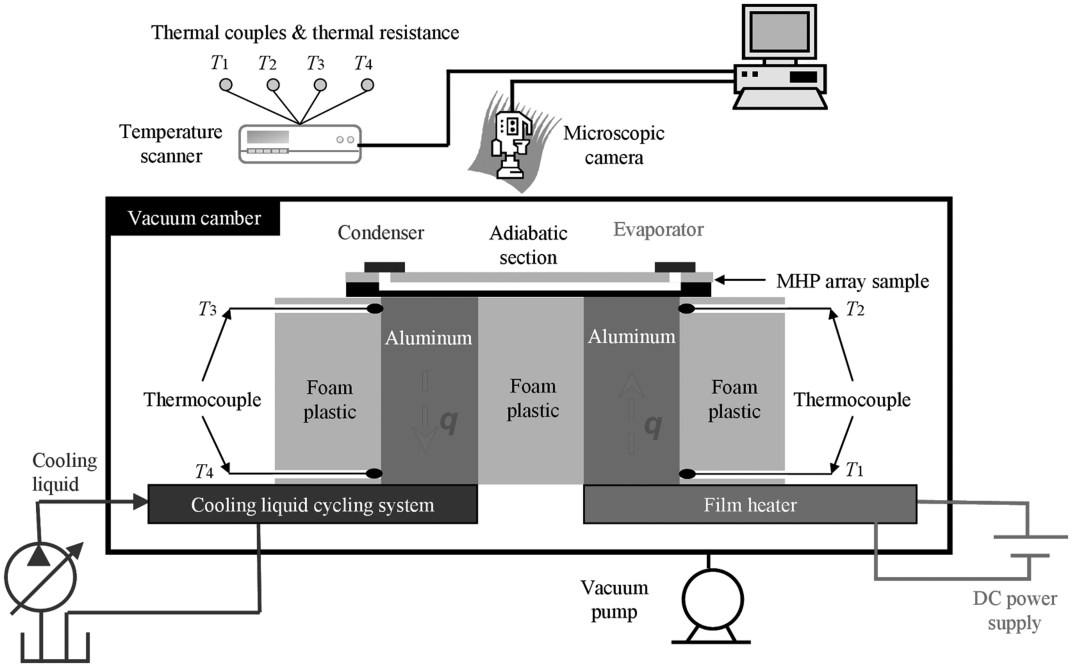

Fig. 5 Schematic diagram of the experimental setup.

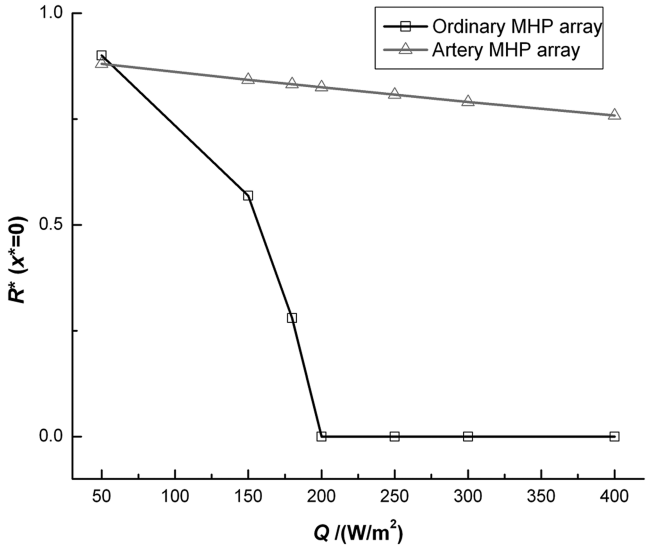

Fig. 6 Variation of the dimensionless radius of meniscus R^* at $x^* = 0$ with different values of heat input of the MHP array.

V. Results and Discussion

A part of the artery MHP array is selected for numerical analysis, which is composed of three equilateral triangular pipes with arteries' width of 100 μm and MHP's width of 200 μm. The width of the ordinary MHP used as reference is 200 μm. Both of the artery MHP and the ordinary MHP are characterized by an equal evaporation length, adiabatic length and condensation length with a total length of 20 mm. Ethanol is selected as the working liquid. These two kinds of MHP are assumed to be working in a horizontal condition ($\beta = 0$). The simulation describes the working states of the liquid, including liquid velocity and radius of the meniscus at different locations in a single V-groove of the MHP.

A. Radius of Meniscus Curvature and Liquid Velocity Gradient with Different Heat Input

The MHP is commonly divided into three sections along the axial direction: evaporator, adiabatic, and condenser. In each section of the MHP, the radius of the meniscus has a direct effect on the flow condition of the working liquid. In an ordinary MHP, the liquid backflow completely depends on the capillary force of the V-grooves. When the input heat, Q, exceeds the critical value, there will not be enough capillary force for the liquid backflow. Then the dryout region will propagate from the hot end, which decreases the heat transfer contact surface between working liquid and the substrate. As shown in Fig. 6, the gradient of the line with rectangle symbols for R^* at $x^* = 0$ change greatly with the input heat. The dryout region will propagate from the hot end, when the input heat increases to 200 W/m^2. However, the artery MHP array can effectively prevent the onset of the dryout region even when the input heat increases to 400 W/m^2. There is just slight change in R^* at $x^* = 0$ of the line with triangle symbols.

Thanks to the existence of the artery, the artery MHP can work well with no concern about the increasing input heat, as shown in Fig. 7a. As the input heat increases, the hot end is still able to be supplied with enough liquid, and the fluctuation range of the line will also increase. The fluctuation range is quite small when compared with the radius curve line of the ordinary MHP with the same heat flux, as shown in Fig. 7b. It leads us to the conclusion that the artery MHP can effectively limit the propagation of the dryout region due to the improvement of its liquid transportation capability.

The working principle of the artery MHP can be further explained with the velocity of the working liquid in the MHP as shown in Fig. 7c. At the hot end ($x = 0$) of the MHP, the velocity of the liquid is negative, as the working liquid is applied by the artery. There are two turning points on the line of dV/dx^* that $V = 0$, each of them present a critical point on the line of dR^*/dx^*. As the input heat increases, the

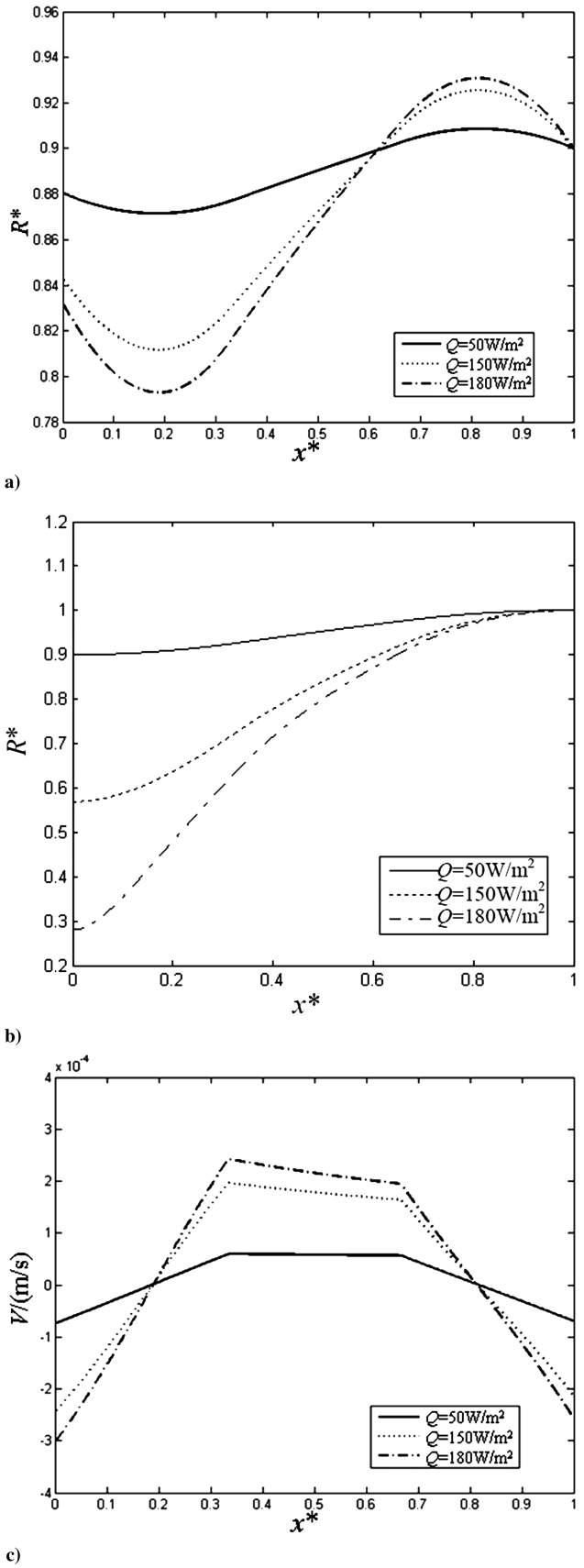

Fig. 7 Comparison simulation on working state of different MHP array with different values of heat input: a) variation of the dimensionless radius of meniscus in artery MHP R^* with dimensionless position x^*, (b) variation of the liquid velocity in the V-grooves of the traditional MHP V with dimensionless position x^*, and c) variation of the liquid velocity in the V-grooves of the artery MHP V with dimensionless position x^*.

liquid velocity at the hot end ($x^* = 0$) is higher, which means the artery supplies more working liquid to the hot end.

B. Radius of Meniscus and Liquid Velocity Gradient in the Artery MHP with Different Fill Charge

Above analysis is based on a single V-groove of the MHP working with an artery. While a MHP with triangle cross section is composed of three V-grooves, the dimensionless radius of meniscus R^* has to be corrected due to the fact that it should not be bigger than 1. Therefore, a new correction coefficient, δ, is introduced in the boundary conditions. The definition of δ is, at $x^* = 1$, $R^* = \delta$.

The correction coefficient has close relationship with the fill charge. As shown in Fig. 7a, the fluctuation of R^* at the radius direction is relatively small, and its form is similar to the sine curve, so it is rational to assume that the average vapor–liquid ratio at every position of MHP in the axial direction is the same as the cold end ($x^* = 1$). The fill charge can be calculate with the vapor–liquid ratio at the cross section at the cold end ($x^* = 1$).

The liquid area in the cross section can be calculated by Eq. (21)

$$A'_L = 3\left[\frac{\delta a \sin(\alpha)}{2\cos(\alpha+\gamma)}\right]^2 B_1 + \frac{\sqrt{3}}{2}(ca)^2 \tag{21}$$

The general area of the cross section can be calculated by Eq. (22)

$$A' = \frac{\sqrt{3}(1+2c^2)a^2}{4} \tag{22}$$

The relationship between the fill charge η and the correction coefficient δ can be described by Eq. (23)

$$\eta = \frac{A'_L}{A'} = \frac{12[\frac{\delta\sin(\alpha)}{2\cos(\alpha+\gamma)}]^2 B_1 + 2\sqrt{3}c^2}{\sqrt{3}(1+2c^2)} \tag{23}$$

The working parameters of the artery MHP under different fill charge are shown in Fig. 8a. When $\delta = 0.95$, the curve line of the dimensionless radius of meniscus, R^*, is below 1. When δ is smaller, which means the MHP is filled with less working liquid; the extremum of the liquid velocity in the V-grooves is higher as shown in Fig. 8b. The higher extremum of the liquid velocity will induce a stronger friction force to obstruct the backflow of working liquid. So a bigger $\delta = 0.9$ is preferred to indicate the fill charge of the artery MHP array.

C. Working-State Observations

The curve of the temperature vs the input heat in the evaporator section of a silicon substrate embedded with artery MHPs is slightly below the one without artery MHPs as shown in Fig. 9. When the temperature of evaporator section reaches about 73°C, which is the boiling point of ethanol, the artery MHP reaches its boiling limit. According to the results shown in Fig. 9, the working temperature range of artery MHP array can be extended to the boiling limit with no concern about the capillary limit. As to the common MHP, it always reaches the capillary limit before reaching boiling limit [19]. It is obvious that the design of artery MHP array can effectively prevent the propagation of dryout region due to availability of enough capillary force.

The working state is recorded with the microscopic camera with amplification factor of 200×. The condenser section of the MHP array maintains a steady temperature, about 25°C, and the evaporator section is heated by a thin film heater. As shown in Fig. 10a, the working liquid in the evaporator section of MHP becomes boiling when the input heat exceeds the critical level. As shown in Fig. 10b, the red rectangles denote the liquid level in V-grooves of the three sections in the arteries. It is obvious that the liquid level changes greatly in the three sections, but the liquid can still be efficiently supplied to the evaporator section. It means that the artery MHP can work well with a relative high heat flux compared with the ordinary MHP array.

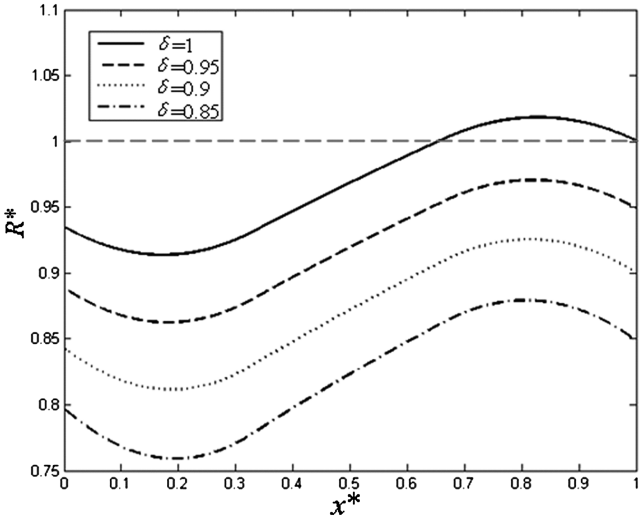

a)

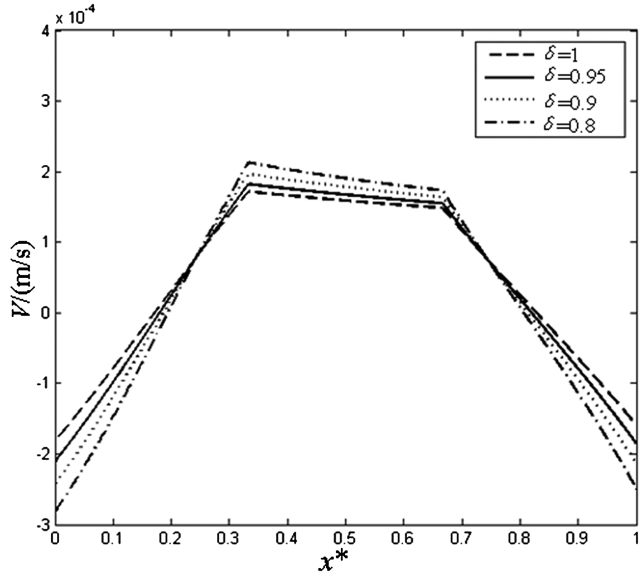

b)

Fig. 8 Working state of the artery MHP array with different values of fill charge rate: a) variation of the dimensionless radius of meniscus in MHP R^* with dimensionless position x^*, and b) variation of the liquid velocity in the V-grooves of the MHP V with dimensionless position x^*.

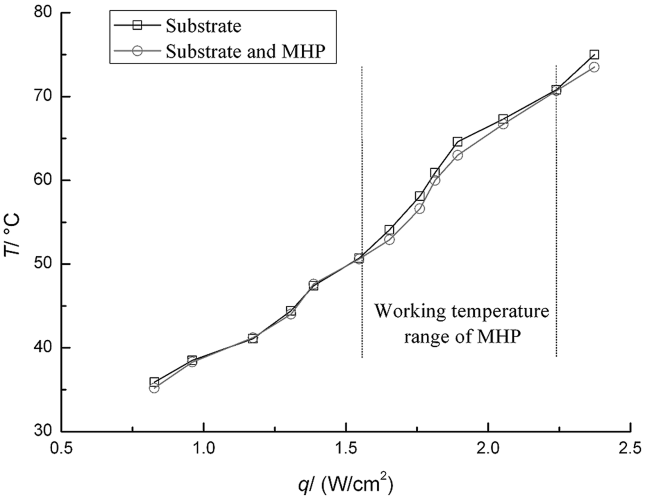

Fig. 9 Temperature of the evaporator section on the artery MHP array with different input heat.

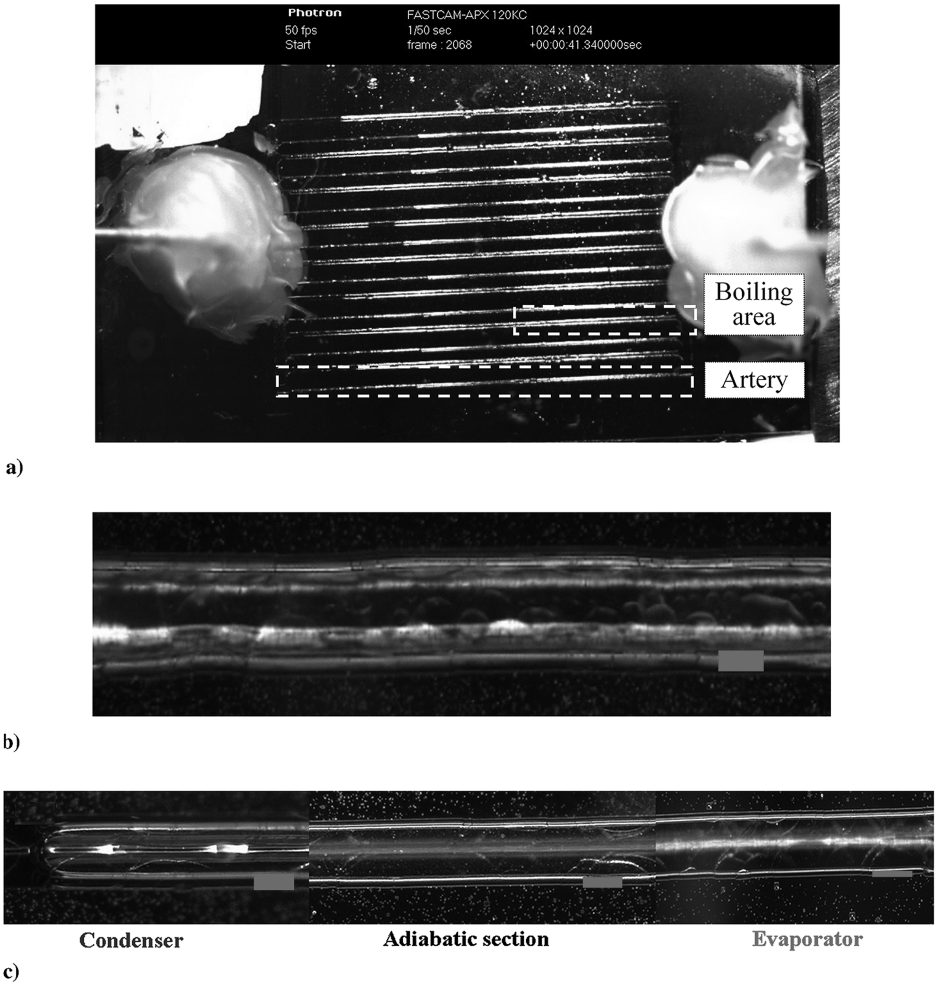

Fig. 10 Photos of artery MHP array: a) working state of the artery MHP array in critical condition, b) boiling area at the hot end of MHP, and c) liquid in the artery.

VI. Conclusions

A one-dimensional steady-state model is built for the novel artery MHP. According to the numerical solution of the model, two conclusions can be obtained: 1) The artery MHP array can effectively supply liquid back to the evaporator section. Thanks to the existence of the arteries, the objective to limit the onset of dryout region is achieved and related better thermal performance such as wide thermal working range is realized. 2) The factor δ, which is related to the fill charge of the artery MHP array, is recommended to be 0.9, under which the optimal fill charge can be obtained.

The sample of artery MHP array is fabricated on the silicon wafer and observed with microscopic camera. The experimental validation of the novel design is carried out by the observation of the novel artery MHP working states. The working state observational results show a good agreement with the assumed working principle.

Acknowledgment

The project was supported by Zhejiang Provincial Natural Science Foundation of China (No. R105008).

References

[1] Cotter, T. P., "Principles and Prospects of Micro-Heat Pipe," *Proceedings of the 5th International Heat Pipe Conference*, Japan Technology and Econ. Center, Inc., Tsukuba, Japan, 1984, pp. 328–332.

[2] Sobhan, C. B., Rag, R. L., and Peterson, G. P., "Comparative Study of the Investigations on Microheat Pipes," *International Journal of Energy Research*, Vol. 31, Nos. 6–7, 2007, pp. 664–688. doi:10.1002/er.1285

[3] Suman, B., Sirshendu, D., and DasGupta, S., "A Model of the Capillary Limit of a Microheat Pipe and Prediction of the Dryout Length," *International Journal of Heat and Fluid Flow*, Vol. 26, No. 3, 2005, pp. 495–505. doi:10.1016/j.ijheatfluidflow.2004.09.006

[4] Suman, B., and Hoda, N., "Effect of Variations in Thermophysical Properties and Design Parameters on the Performance of a *V*-Shaped Micro Grooved Heat Pipe," *International Journal of Heat and Mass Transfer*, Vol. 48, No. 10, 2005, pp. 2090–2101. doi:10.1016/j.ijheatmasstransfer.2005.01.007

[5] Berre, M. L., Launay, S., Sartre, V., and Lallemand, M., "Fabrication and Experimental Investigation of Silicon Microheat Pipes for Cooling Electronics," *Journal of Micromechanics and Microengineering*, Vol. 13, No. 3, 2003, pp. 436–441. doi:10.1088/0960-1317/13/3/313

[6] Kang, S. W., and Huang, D., "Fabrication of Star Grooves and Rhombus Grooves Microheat Pipe," *Journal of Micromechanics and Microengineering*, Vol. 12, No. 5, 2002, pp. 525–531. doi:10.1088/0960-1317/12/5/303

[7] Thomas, Scott, K., and Damle, Vikrant, C., "Fluid Flow in Axial Reentrant Grooves with Application to Heat Pipes," *Journal of Thermophysics and Heat Transfer*, Vol. 19, No. 3, 2005, pp. 395–405. doi:10.2514/1.10711

[8] Chen, Y., Zhang, C., Shi, M., Wu, J., and Peterson, G. P., "Study on Flow and Heat Transfer Characteristics of Heat Pipe with Axial Omega-Shaped Microgrooves," *International Journal of Heat and Mass Transfer*, Vol. 52, Nos. 3–4, 2009, Nos. 3–4, pp. 636–643. doi:10.1016/j.ijheatmasstransfer.2008.08.003

[9] Chen, Y., Zhu, W., Zhang, C., and Shi, M., "Thermal Characteristics of Heat Pipe with Axially Swallow-tailed Microgrooves," *Chinese Journal of Chemical Engineering*, Vol. 18, No. 2, 2010, pp. 185–193. doi:10.1016/S1004-9541(08)60341-9

[10] Kang, S. W., Tsai, S. H., and Ko, M. H., "Metallic Microheat Pipe Heat Spreader Fabrication," *Applied Thermal Engineering*, Vol. 24, Nos. 2–3, 2004, pp. 299–309.

doi:10.1016/j.applthermaleng.2003.08.008
[11] Qu, J., Wu, H. Y., and Cheng, P., "Effects of Functional Surface on Performance of a Microheat Pipe," *International Communications in Heat and Mass Transfer*, Vol. 35, No. 5, 2008, pp. 523–528. doi:10.1016/j.icheatmasstransfer.2007.10.001
[12] Yoshihiro, I., Heydari, M., and Hashimoto, A., "The Movement of a Water Droplet on a Gradient Surface Prepared by Photodegradation," *Langmuir*, Vol. 23, No. 4, 2007, pp. 1845–1850. doi:10.1021/la0624992
[13] Nakayama, G., and Cheng, P., "Effects of Interface Wettability on Microscale Flow by Molecular Dynamics Simulation," *International Journal of Heat and Mass Transfer*, Vol. 47, No. 3, 2004, pp. 501–513. doi:10.1016/j.ijheatmasstransfer.2003.07.013
[14] Suman, B., "A Steady State Model and Maximum Heat Transport Capacity of an Electrohydrodynamically Augmented Micro-Grooved Heat Pipe," *International Journal of Heat and Mass Transfer*, Vol. 49, Nos. 21–22, 2006, pp. 3957–3967. doi:10.1016/j.ijheatmasstransfer.2006.04.011
[15] Kim, S. J., Seo, J. K., and Do, K. H., "Analytical and Experimental Investigation on the Operational Characteristics and the Thermal Optimization of a Miniature Heat Pipe with a Grooved Wick Structure," *International Journal of Heat and Mass Transfer*, Vol. 46, No. 11, 2003, pp. 2051–2063. doi:10.1016/S0017-9310(02)00504-5
[16] Lin, Y. H., Kang, S. W., and Wu, T. Y., "Fabrication of Polydimethylsiloxane (PDMS) Pulsating Heat Pipe," *Applied Thermal Engineering*, Vol. 29, Nos. 2–3, 2009, pp. 573–580. doi:10.1016/j.applthermaleng.2008.03.028
[17] Launay, S., Sartre, V., and Lallemand, M., "Experimental Study on Silicon Micro-Heat Pipe Arrays," *Applied Thermal Engineering*, Vol. 24, Nos. 2–3, 2004, pp. 233–243. doi:10.1016/j.applthermaleng.2003.08.003
[18] Ayyaswamy, P. S., Catton, I., and Edwards, D. K., "Capillary Flow in Triangular Grooves," *Journal of Applied Mechanics*, Vol. 41, 1974, pp. 332–336.
[19] Peterson, G. P., "Heat Pipe Modeling and Simulation," *AIAA 23rd Aerospace Sciences Meeting*, AIAA, Reston, VA, Jan. 1985.